PAPER • OPEN ACCESS

Co- and contra-directional vertical coupling between ferromagnetic layers with grating for short-wavelength spin wave generation

New Journal of Physics
The open access journal at the forefront of physics

Deutsche Physikalische Gesellschaft DPG
IOP Institute of Physics

Published in partnership with: Deutsche Physikalische Gesellschaft and the Institute of Physics

OPEN ACCESS

RECEIVED
16 November 2017

REVISED
26 March 2018

ACCEPTED FOR PUBLICATION
3 April 2018

PUBLISHED
9 May 2018

PAPER

Co- and contra-directional vertical coupling between ferromagnetic layers with grating for short-wavelength spin wave generation

Piotr Graczyk[1], **Mateusz Zelent** and **Maciej Krawczyk**

Faculty of Physics, Adam Mickiewicz University in Poznan, Umultowska 85, 61-614 Poznan, Poland
[1] Author to whom any correspondence should be addressed.

E-mail: graczyk@amu.edu.pl **and** krawczyk@amu.edu.pl

Keywords: magnonics, magnetization dynamics, directional couplers, spin waves

Abstract

The possibility to generate short spin waves (SWs) is of great interest in the field of magnonics nowadays. We present an effective and technically affordable way of conversion of long SWs, which may be generated by conventional microwave antenna, to the short, sub-micrometer waves. It is achieved by grating-assisted resonant dynamic dipolar interaction between two ferromagnetic layers separated by some distance. We analyze criteria for the optimal conversion giving a semi-analytical approach for the coupling coefficient. We show by the numerical calculations the efficient energy transfer between layers which may be either of co-directional or contra-directional type. Such a system may operate either as a short spin wave generator or a frequency filter, moving forward possible application of magnonics.

1. Introduction

Smaller is better. This paradigm is a driving force in many modern branches of applied physics and technology. The advances in miniaturization of silicon-based logic devices have followed famous Moores law to the 1990s [1]. Now, the dimensions and operating voltages in CMOS technology are pushed to the limits. Therefore, new ideas for memory and logic devices are desirable and some have already been emerged [2].

Some of the novel concepts come from magnonics, which is promising for processing information field of modern magnetism [3–5]. Magnonics deals with the spin waves (SWs) as a carrier of information and thus it is expected to combine high frequency and short-wavelength together with low power consumption [6–8]. The possibility of miniaturization of spin-wave-based logic devices is dependent on the wavelength, thus the attention is focused on searching the ways of generation of short SWs. Several approaches has been recently reported: shortening the wavelength in a tapered waveguide [9], microwave-to-SW transducers based either on magnetic wires [10], nanostructure edges [11], diffraction gratings [12–14], coplanar waveguides [15] or anisotropy-modulated multiferroic heterostructures [16], transduction of acoustic waves into short SWs due to magneto-elastic coupling [17, 18], and emitters based on current-driven oscillating pinned domain walls [19].

The SW waveguides, multiplexers [20], coupled waveguides with or without exploitation of periodic gratings [21–23] have been investigated as basic units for processing information, some of them were demonstrated experimentally. Most of these studies deal with the in-plane SW propagation, but control of SW propagation in out of-plane direction is also promising for applications, although an area of 3D magnonics still remain unexplored [24]. Multilayer structures have already been studied for controlling SW spectra in thin films with using periodic gratings [25–27], periodic gratings were also used to excite and detect SWs propagating in homogeneous film beneath it. However, the way of transferring of the SW energy in the vertical direction has not yet been established.

In this paper we investigate the effect of grating-assisted directional coupling between SWs propagating in two ferromagnetic layers. We formulate phenomenological expression for the coupling strength and discuss a co-directional and contra-directional couplings between the layers, which allow for a transfer energy between them. The conditions for efficient resonant coupling are defined. In numerical simulations we consider

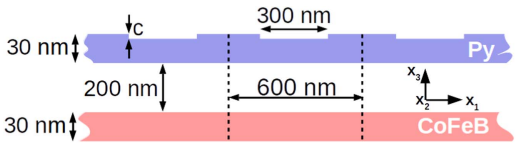

Figure 1. The scheme of considered bilayer system composed of CoFeB film and Py film with the periodically corrugated surface. Dashed lines indicate the unit cell.

permalloy (Py)-CoFeB bilayer separated by a nonmagnetic spacer, with Py layer decorated with a grating. We show, that it is possible to achieve complete SW power exchange between the layers, if the structure is optimized for resonant, phase-matched interaction of a proper magnitude. We tested influence of damping on the SW energy exchange between layers, and show that the effect can be optimized by increasing grating thickness. We propose such a system to be a simple and efficient transducer for generation of short SWs in Py from long SWs in CoFeB, which allows to transfer the SW signals in the vertical direction, and also to exploit it as a narrow band filters for future magnonic devices.

2. The model and the methods

2.1. Optimization of coupling strength

The phenomenon of coupling and energy exchange between two identical uniform ferromagnetic films has already been discussed [28, 29] and it was shown with Brillouin light spectroscopy (BLS) for side coupling between two waveguides two years ago [22]. Recently, application of that effect, widely used in photonics from many years [30, 31], has been proposed for signal processing with two coupled magnonic waveguides [32]. In this case, the resonant interaction between SWs propagating in the identical waveguides exists in relatively wide range of frequencies if the distance between them is properly tuned. If the layers are different, the SWs are decoupled and each wave becomes confined to a single layer. However, the existence of the other layer still affects the dispersion of the SWs in a range of frequencies. We can couple them again by introducing the periodicity of the structure. Folding of the bands to the Brillouin zone will result in multiple crossings of the bands that originate from different layers. Then, by tuning the distance between layers, to ensure that crossings lie in the frequency region of strong interaction between layers, we can achieve strong hybridization between the SW bands. To sum up, the criteria of efficient power exchange between different ferromagnetic media (waveguides or layers) are the following: (1) the resonance, i.e. the equality of the frequencies, (2) phase matching—equality of the wavevectors, and (3) strong interaction between layers.

For the efficient energy exchange between SWs in the coupling-in-space mechanism, it is crucial to choose materials with low damping. The best candidates are yttrium iron garnet (YIG) and CoFeB. However, due to the extremely high magnetic contrast between that materials, it is difficult to match all three conditions: the wavelength of the SW in YIG is much shorter than in CoFeB at the same frequency, and it is the wave mainly driven by the exchange interaction. As a result, the mode in YIG creates very weak stray magnetic field around and the layers must be in an unfeasibly close distance to couple. Due to this, we have chosen Py and CoFeB as materials of significant contrast, but small enough to ensure high stray fields for both SW modes.

Considered bilayer system (figure 1) consists of CoFeB 30 nm thick homogeneous film and 30 nm Py film. Py is patterned periodically with grooves of 300 nm width and the depth of either 5 nm (Py5) or 15 nm (Py15). The grating has the lattice constant 600 nm. Such dimensions make the structure feasible for fabrication and SW detection achievable by conventional techniques, such as BLS or SW spectroscopy. We assume, that the layers are infinite along the x_2-coordinate. The separation between layers has been optimized for the sufficient strong interaction at the points of lowest band crossings (discussed latter) and its value is fixed to 200 nm.

To study coupling in the bilayered structure the Landau–Lifshitz–Gilbert equation has been solved either in frequency-domain (for calculation of the dispersion relations) or in the time-dependent computations, both with the use of COMSOL Multiphysics. The details of calculations are described in [33]. We assumed for the CoFeB (Py) layer the values of the exchange constant of 15 pJ m^{-1} (13 pJ m^{-1}), of the saturation magnetization $M_s = 1250$ kA m^{-1} (860 kA m^{-1}) and the damping $\alpha = 0.004$ (0.01). The layers are assumed to be saturated in the x_2 direction by the external magnetic field $H_0 = 40$ kA m^{-1}. The results of finite element method have been verified by the micromagnetic simulations performed with MuMax3 [34], which was also used to estimate effectiveness of the SW transfer between the layers and to test filtering properties.

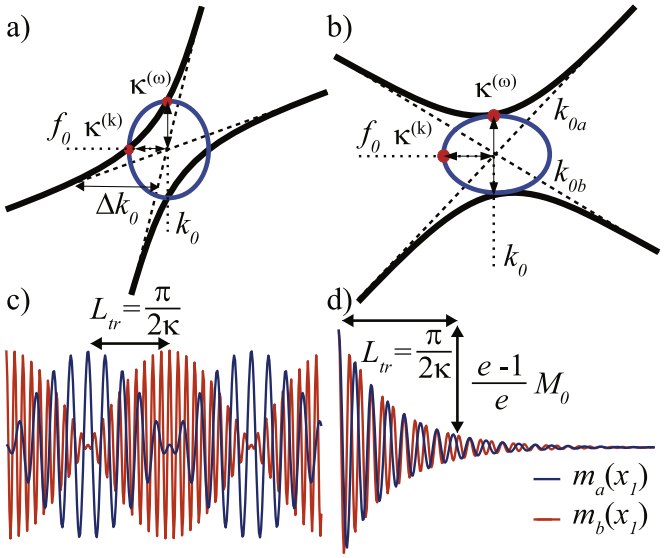

Figure 2. Possible couplings between SWs in the bilayered structure with periodicity and the definition of characteristic values. (a) Hybridization in co-directional coupling, (b) hybridization in contra-directional coupling, (c) spatial SW amplitude distribution in the case of co-directional coupling, and (d) spatial amplitude distributions in the case of contra-directional coupling.

2.2. Coupled mode theory formalism

Before presenting the numerical results, we formulate an approach for calculation the coupling between SWs propagating in two different ferromagnetic layers, *a* and *b*, which is based on the coupled mode theory widely used in electromagnetism [35, 36]. A dynamic magnetization $\vec{m}_a$ of the SW mode in the layer *a* is under influence of the magnetic stray field $\vec{h}_b$ generated by the SW $\vec{m}_b$ in the layer *b*. The energy of this interaction is

$$E_{ba} = \frac{1}{S}\int \vec{m}_a^* \cdot \vec{h}_b \mathrm{d}S, \tag{1}$$

where integration is conducted through the area *S* of the unit cell of the structure (see, figure 1). The fields are normalized according to

$$\frac{1}{S}\int \vec{m}_i^* \cdot \vec{h}_i \mathrm{d}S = 1, \tag{2}$$

where $i = a, b$. The power transferred from the layer *b* to the layer *a* at the angular frequency ω is given by

$$\kappa_{ba}^{(\omega)} = \frac{1}{S}\int \frac{\partial \vec{m}_a^*}{\partial t} \cdot \vec{h}_b \mathrm{d}S = \mathrm{i}\omega \frac{1}{S}\int \vec{m}_a^* \cdot \vec{h}_b \mathrm{d}S. \tag{3}$$

The coupling coefficient $\kappa_{ab}^{(\omega)}$ which describes energy flow from medium *a* to *b* is defined similarly. This formula allows to estimate coupling strength between two waveguides knowing the distributions of stray fields $\vec{h}_i$ and related SW amplitudes $\vec{m}_i$ of the separated layers. As $\kappa^{(\omega)} \equiv |\kappa_{ab}^{(\omega)}| = |\kappa_{ba}^{(\omega)}|$ is a periodic function of the coordinate in grating-assisted coupler [37], the formula (3) describes an average value of the coupling coefficient in the unit cell. The value of the coupling coefficient $\kappa^{(\omega)}$ defines also the width of the band splitting in a dispersion relation in the frequency scale (figure 2). We can express coupling coefficient also in the wavevector scale by

$$\kappa \equiv \kappa^{(k)} = \kappa^{(\omega)}/v, \tag{4}$$

where $v = (v_a + v_b)/2$, and v_a is the group velocity of SW in the layer *a* and v_b in the layer *b*. It is assumed that group velocities are constant close to the modes crossing (in the absence of coupling). By this reformulation of the coupling coefficient from the frequency to the wavevector scale, it is possible to describe the coupled modes at a resonant frequency f_0 as a sum of two modes which wavenumbers differ by $\Delta k = 2\kappa$ and one of them is symmetric while the other is antisymmetric. Due to the periodicity in the structure and the folding-back effect the two family of bands (these related to SWs in *a* and *b* layers) cross each other. The crossing bands can have the same (figure 2(a)) or opposite (figure 2(b)) sign of the group velocity. In the first case we call them co-directional and in the second contra-directional couplings.

Considering co-directional coupling (figure 2(a)) at a resonance frequency $f_0 = \omega_0/2\pi$, the sum of these two waves in the medium *a* is

$$m_a(x,\ t) \propto \mathrm{e}^{\mathrm{i}\omega t}[\mathrm{e}^{\mathrm{i}k_a x} + \mathrm{e}^{\mathrm{i}k_b x}] = 2\mathrm{e}^{\mathrm{i}(k_0 x - \omega t)}\cos(\kappa x), \tag{5}$$

with k_a and k_b being wavevectors in sublayer a and b respectively, while in medium b it is

$$m_b(x,\ t) \propto \mathrm{e}^{\mathrm{i}\omega t}[\mathrm{e}^{\mathrm{i}k_a x} - \mathrm{e}^{\mathrm{i}k_b x}] = 2\mathrm{e}^{\mathrm{i}(k_0 x - \omega t)}\sin(\kappa x), \tag{6}$$

where the relative amplitudes were omitted for simplicity. If $\kappa \ll k_0$, i.e. in the weak coupling regime, the interference of that two modes results in the effect of beating with the spatial frequency defined by $\kappa^{(k)}$ (figure 2(c)).

For the $f \neq f_0$, i.e., for $k_a,\ k_b \neq k_0$, the value of κ may be read from dispersion relations (figure 2) as $\kappa = k_{0a} - k_a = k_b - k_{0b}$. The exact solutions for the boundary conditions $|m_a(0,\ t)| = M_0$ (M_0 being maximal SW amplitude), $|m_b(0,\ t)| = 0$ are [36]

$$\begin{aligned} m_a(x,\ t) &= M_0\left(\cos(Bx) - \mathrm{i}\frac{\Delta k_0}{B}\sin(Bx)\right)\mathrm{e}^{-\mathrm{i}\bar{k}_0 x}\mathrm{e}^{\mathrm{i}\omega t}, \\ m_b(x,\ t) &= M_0\frac{\kappa}{B}\sin(Bx)\mathrm{e}^{-\mathrm{i}\bar{k}_0 x}\mathrm{e}^{\mathrm{i}\omega t}, \end{aligned} \tag{7}$$

where $\Delta k_0 = (k_{0a} - k_{0b})/2$, $\bar{k}_0 = (k_{0a} + k_{0b})/2$, and $B = \sqrt{\Delta k_0^2 + \kappa^2}$.

In case of contra-directional coupling (figure 2(b)) at a resonance frequency f_0, the value of κ becomes imaginary at the vicinity of crossing. The wave is a sum of two modes $k_1 = k_0 + \mathrm{i}\kappa$ and $k_2 = -k_0 + \mathrm{i}\kappa$ which propagate at opposite directions. If we suppose that initially the input wave exists only at the medium a, i.e., $a(x = 0) \neq 0$ and $b(x \to \infty) = 0$ then we can write expressions for a and b in the simplified form as [36]

$$\begin{aligned} m_a(x,\ t) &\propto \mathrm{e}^{-\kappa x}\cos(k_0 x - \omega t), \\ m_b(x,\ t) &\propto \mathrm{e}^{-\kappa x}\sin(k_0 x - \omega t). \end{aligned} \tag{8}$$

The resulting effect is a Bragg reflection: the amplitude of wave a is a decaying function of x (figure 2(d)) and the outgoing wave b propagates in the opposite direction.

The exact solution for $f \neq f_0$ with the substitution $T = \mathrm{i}B$ and the boundary conditions $|m_a(0,\ t)| = M_0$ and $|m_b(0,\ L)| = 0$, i.e. when the SW mode in the layer b is supposed to have zero amplitude at the distance L is

$$\begin{aligned} m_a(x,\ t) &= M_0\frac{\cosh Tx - \frac{\kappa^2}{T^2}\sinh TL\sinh T(x - L) - \mathrm{i}\frac{\Delta k_0}{T}\sinh Tx}{1 + \frac{\kappa^2}{T^2}\sinh TL}\mathrm{e}^{-\mathrm{i}\bar{k}_0 x}\mathrm{e}^{\mathrm{i}\omega t}, \\ m_b(x,\ t) &= M_0\frac{\kappa}{T}\frac{\cosh TL\sinh T(x - L) - \mathrm{i}\frac{\Delta k_0}{T}\sinh TL\sinh T(x - L)}{1 + \frac{\kappa^2}{T^2}\sinh TL}\mathrm{e}^{-\mathrm{i}\bar{k}_0 x}\mathrm{e}^{\mathrm{i}\omega t}. \end{aligned} \tag{9}$$

With the damping neglected, the efficiency of the energy transfer from the layer a (CoFeB film) to the layer b (Py film) and vice-versa is described in the coupled mode formalism by energy transfer efficiency coefficient:

$$A^2 = \frac{\kappa^2}{B^2}, \tag{10}$$

which is equal to the ratio of the maximum square amplitudes of the waves in the layers. Energy transfer efficiency coefficient decreases as the value of κ decreases (i.e., out of the resonance) and it also decreases with the increase of phase mismatch Δk_0.

The energy transfer depends also on damping. To estimate its influence, we introduce a damping to our coupled mode calculations by introducing complex wavevectors $k_{0a,0b} = k^r_{0a,0b} + \mathrm{i}k^i_{0a,0b}$ to the exact solutions of the coupled modes, equations (7) and (9). The values of k^i are calculated from the formulas for surface SW lifetime τ and group velocity v [38]:

$$k^i = \frac{1}{v\tau} = \frac{4\omega\alpha}{\omega_M^2 d}(\omega_0 + 0.5\omega_M)\mathrm{e}^{2k^r d}, \tag{11}$$

where $\omega_0 = \gamma\mu_0 H_0$, $\omega_M = \gamma\mu_0 M_s$ and d is layer thickness. The complex values of k_{0a} and k_{0b} in the co-directional coupling lead to: (1) decrease of the maximum amplitude of SWs and (2) the shift of the distance at which the wave transferred from layer a to the layer b reaches its maximum amplitude. Then, we define the energy transfer efficiency coefficient from the layer a to the layer b for co-directional coupling as [36]

$$A^2 = \frac{|m_b(x_{\max})|^2}{|m_a(0)|^2}, \tag{12}$$

where $x_{\max}$ is the first intensity maximum in the layer b. For contra-directional coupling, we compare the square amplitude at the output of the layer b to the square amplitude at the input of the layer a:

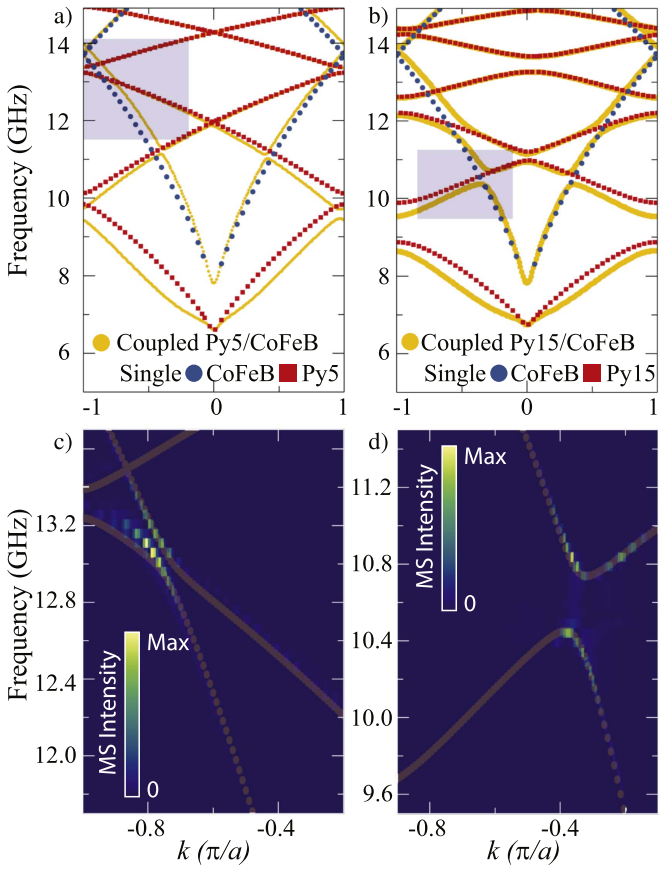

Figure 3. Dispersion relations of (a) Py5 (5 nm deep groves)/CoFeB and (b) Py15/CoFeB bilayers (yellow dots) from COMSOL simulations. Dispersions of single Py5, Py15 and CoFeB layers are also indicated. In (c) and (d) the dispersion at the vicinity of the analyzed crossings are shown and superimposed on the results of micormagnetic simulations (color map).

$$A^2 = \frac{|m_b(0)|^2}{|m_a(0)|^2}. \tag{13}$$

3. Results

Figure 3(a) shows the dispersion relation for the Py5/CoFeB system (see the yellow dots). Blue and red dots indicate dispersion relations of the isolated Py film with 5 nm deep groves (Py5) and CoFeB films, respectively. It is seen from the plot, that the dispersion of bilayered structure differs from the dispersions of isolated films at a range of frequencies. For k close to zero the frequencies for Py5/CoFeB are the same as for separate films, because the stray fields are absent for homogeneous excitation and weak in long-wavelength limit. On the other hand, for high values of k dispersion reaches exchange regime and stray fields become also weak. Between that two limits there exists a region of strong interaction.

The effect of nonreciprocity is also apparent from figure 3(a) for the bilayered structure. It is manifested both, by a difference in the frequency of the waves at $+k$ and $-k$, as well as the differences in the coupling strength on both sides of the Brillouin zone center. Clearly, hybridization at crossings for the $-k$ are stronger than for the positive values of k. These effects are due to nonreciprocity of the Damon–Eshbach mode and the asymmetry of the structure [27, 39].

The branches which originate from the dispersions of two different films anti-crosses at some k points. Thus, choosing appropriate crossing points in the region of strong interaction, we can fulfill the criteria of resonance and phase matching for that waves, required for SW power exchange between the layers. For the time domain investigation described below we have chosen crossings at 13 GHz (for co-directional coupling) and 10.6 GHz (for contra-directional coupling) presented in figures 3(c) and 3(d), respectively.

3.1. Co-directional coupler

The line source of the wave in time domain simulations is placed at $x_1 = 28$ μm in the CoFeB film. CoFeB film exists along the whole x_1-range, while Py spreads out from $x_1 = 0$ to $x_1 = 25$ μm. The corrugation of Py film

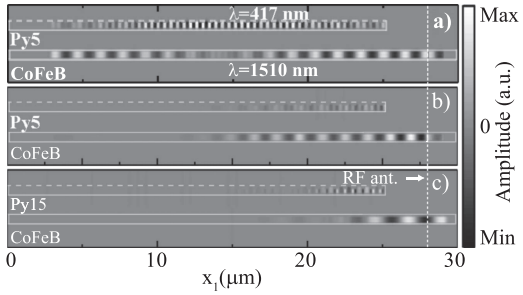

Figure 4. Spatial distribution of the magnetization component m_{x1} after 15 ns of sinusoidal excitation by RF antenna in: (a) Py5/CoFeB without damping, (b) Py5/CoFeB with damping, (c) Py15/CoFeB with damping. Lines indicate boundaries of the layers, dashed line indicates periodic surface of the Py layer.

(stripe hole depth) is here $c = 5$ nm (Py5). Strong damping close to the both ends of CoFeB and left end of Py is introduced to prevent reflections. Figure 4(a) shows magnetization component m_1 after 15 ns of excitation. The amplitude of the SW which goes to the left is decreasing from the maximum value at $x_1 > 25$ μm to almost zero at $x_1 = 14.5$ μm. Its wavelength is 1.51 μm. At the same distance, the SW in Py appears to reach maximum amplitude at $x_1 = 14.5$ μm. Therefore, the energy of the wave in CoFeB has been vertically transformed into the energy of the wave in Py5 completely at a distance of 10.4 μm. Wave induced in Py has the wavelength of 417 nm, that is almost 4 times shorter than those which excites it.

The coupling coefficient read out from the dispersion relation (figure 3(a)) is $\kappa = 0.131$ μm^{-1} which gives the value of transfer length $L_{tr} = \pi/2\kappa = 11.9$ μm, it is a little longer than obtained from time-dependent simulations. The same coupling coefficient calculated from equation (3) gives the value of 0.145 μm^{-1} and thus $L_{tr} = 10.9$ μm.

When the damping is introduced, the effect of energy exchange between layers is strongly suppressed. As it is shown in figure 4(b), the short wave in Py5 is still excited by the wave in CoFeB, but neither clear maximum amplitude in Py nor corresponding minimum in CoFeB are visible. The damping length for Py film is of about 2–3 μm, thus it is much smaller than the length at which transfer from CoFeB occurs. At a given distance, Py film looses more energy than it gets from CoFeB and full transfer of energy and its accumulation cannot take place.

We can recover accumulation of energy in Py layer with damping by increasing coupling coefficient between layers. For this purpose we increase the corrugation depth of Py to $c = 15$ nm (Py15). The dispersion relation for Py15/CoFeB is shown in figure 3(b). It is clearly seen, that the separation between branches increased significantly at the poins of crossings, which indicates increase of coupling strength. The calculated value of κ (equations (3) and (4)) is 0.58 μm^{-1} which gives $L_{tr} = 2.7$ μm. Note that the resonant frequency f_0 is 11.9 GHz for the Py15/CoFeB.

The time-dependent simulations are presented in figure 4(c). The wave in CoFeB vanish much faster with the distance, because it transfers the energy to Py in shorter time. The excited wave in Py grows and the amplitude reaches maximum value at $x_1 = 23$ μm. Therefore, the energy is clearly accumulated in Py despite damping. At further distance it is seen that small amount of energy is transferred back to CoFeB and again back to Py15.

3.2. Contra-directional coupler

The crossing shown in figure 2(b) from the dispersion relation in figure 3(b) at 10.6 GHz represents contra-directional coupling between SWs in CoFeB and Py of 15 nm deep grooves. The coupling strength estimated from dispersion relation is 0.476 μm^{-1}, while the calculated from the equation (3) based on the stray field amplitude and the magnetization amplitude is 0.435 μm^{-1}, that gives the transfer lengths of 3.34 μm and 3.6 μm, respectively.

We performed time domain simulations with the 10.6 GHz excitation at the source line in the system similar to the discussed above for co-directional coupling. The difference is that we introduced the fragment of the homogeneous Py layer at the x_1 between 20 and 25 μm with the strong damping close to the right edge. This allows us to observe the wave going out of the periodic structure toward the right direction.

Figure 5(a) shows the results of simulations after 5 ns of excitation. Clearly, the wave of the wavelength of about 700 nm is excited in Py15 by the wave of the wavelength 3.85 μm in CoFeB. However, the amplitudes of both waves decay with the distance. The distance at which amplitude decreases by the factor 1/e is about 4 μm. At the output (homogeneous part of Py) we observe the wave which propagates to the right, as shown in figure 5(a). Therefore, the energy of the wave in CoFeB which propagates to the left has been vertically transferred to the energy of the wave in Py, which propagates to the right.

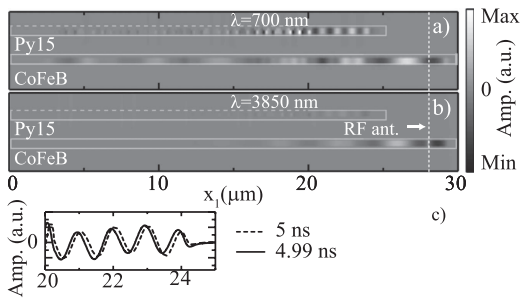

Figure 5. Spatial distribution of the m_{x1} component after 5 ns of sinusoidal excitation at 10.6 GHz by antenna (marked with the dashed vertical line) in: (a) Py15/CoFeB without damping, (b) Py15/CoFeB with damping. Lines indicate boundaries of the layers, dashed line indicate periodic surface of Py layer. (c) m_{x1} in the two consecutive time intervals in the region of uniform Py layer.

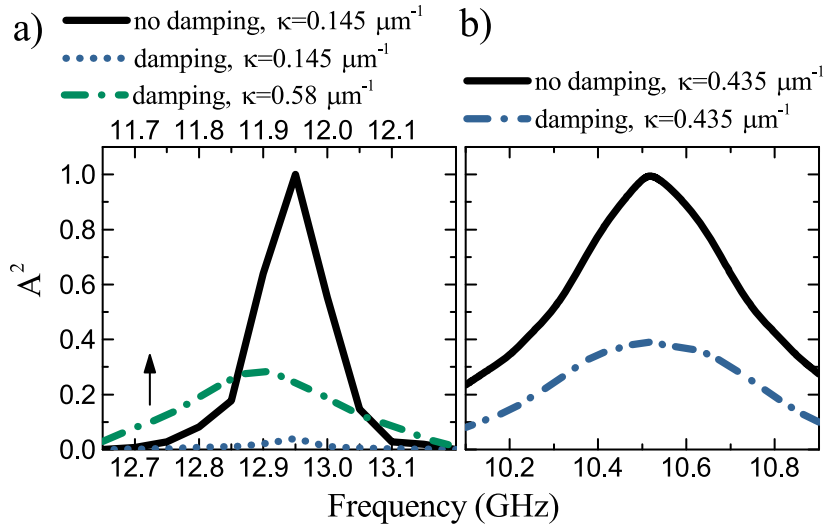

Figure 6. Dependence of the energy transfer efficiency coefficient A^2 on the frequency around resonant frequencies f_0 for (a) co-directional coupling and (b) contra-directional coupling. The results of calculation without (black-solid line) and with damping included for strong ($\kappa = 0.58\ \mu\text{m}^{-1}$, green dotted line) and weak ($\kappa = 0.145\ \mu\text{m}^{-1}$, blue dash–dotted line) couplings are shown.

With the damping introduced (figure 5(b)), the amplitudes of both waves in Py15 and CoFeB decrease. The amplitude of the outgoing wave in Py is also suppressed. However, the transfer of SW from CoFeB to Py film is still visible.

3.3. Energy transfer efficiency

The excitation of the SWs in Py film by a wave propagating in CoFeB is a resonant effect, thus it occurs at maximal efficiency at the particular frequency f_0. The efficiency decreases with moving far away from f_0 and also is suppressed by the damping, always present in the ferromagnetic film. To elucidate influence of those two effects on the transfer efficiency we use the model presented in section 2.2. The efficiency of the energy transfer (A^2) from CoFeB to Py film determined from equation (10) for the case without damping, from equation (12) for co-directional crossing with damping, and from equation (13) for contra-directional crossing with damping, are shown in figure 6.

Figure 6(a) shows A^2 as the function of frequency for the co-directional coupling. Without damping (black-solid line), the efficiency of the energy transfer is 1 at $f_0 = 12.95$ GHz. The energy is transferred completely from a wave of wavelength $\lambda = 1510$ nm in CoFeB layer to the wave of $\lambda = 417$ nm in permalloy (Py5) at a distance of about 11 μm. As the frequency is changed, the efficiency decreases as the consequence of decoupling and phase mismatch (an asynchronous state). With damping taken into account, the efficiency of the process goes down to only 0.04 at resonance (blue-dotted line). The efficiency is increased to 0.3 at the resonance for Py with deeper groves, i.e., in the Py15/CoFeB structure, where the coupling coefficient reaches value of 0.58 μm^{-1} at $f_0 = 11.9$ GHz. For the contra-directional crossing with resonance at $f_0 = 10.5$ GHz (in Py15/CoFeB), the energy transfer efficiency is 1 for the synchronous state without damping at f_0. It decreases when moving the

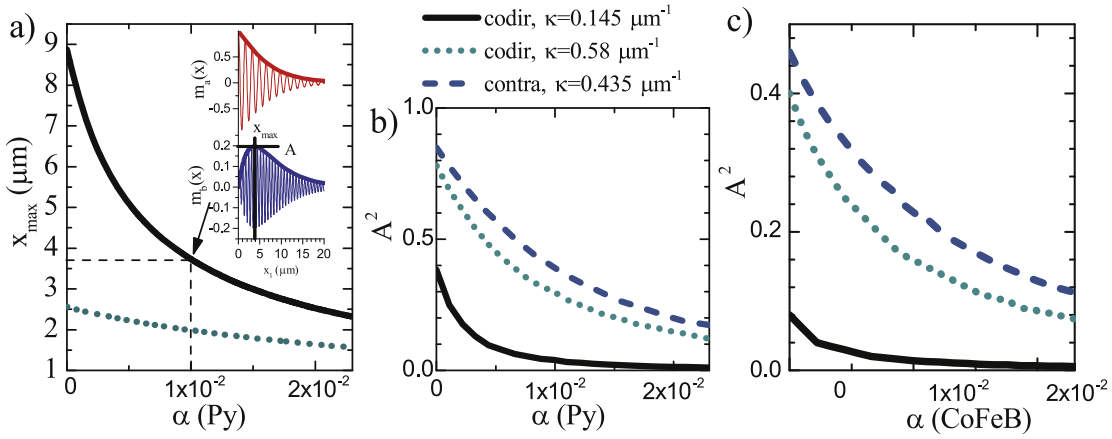

Figure 7. (a) The dependence of the distance at which the wave in Py reaches maximum energy on the damping parameter of Py in co-directional coupling. Dashed lines indicate the value of x_{max} for the value of damping assumed in the rest of calculations. Insets show stationary distribution of $m_a(x)$ and $m_b(x)$ calculated from equations (7) and the definition of A and x_{max}. (b) and (c): The dependencies of energy transfer efficiency on the damping in (b) the Py layer and (c) CoFeB layer for co-directional and contra-directional coupling. The results for weak ($\kappa = 0.145\ \mu m^{-1}$) and strong ($\kappa = 0.58$ and $0.435\ \mu m^{-1}$) couplings are shown.

frequency out of the resonance (see, figure 6(b), solid line). The damping decreases maximum energy reached in Py to almost 40 percent of the initial energy in CoFeB at the resonance (green dash–dotted line).

Interestingly, the damping in the structure does not decrease the efficiency only, but also shifts the position of the maximum amplitude in the case of co-directional coupling. This results, that for no damping the maximum amplitude is reached at $L_{tr} \approx 11\ \mu m$, while with the damping it is for $x_{max} = 3.7\ \mu m$ (both for Py5/CoFeB).

Patterning of the Py film may results on deterioration of its magnetic properties, especially, the process may increase magnetic losses. Therefore, we performed analysis of the transfer efficiency between the layers as a function of Py damping parameter, α_{Py}, keeping the value of α in CoFeB constant. In figure 7(a) the dependence of the distance x_{max} at which the wave excited at f_0 in Py by the wave in CoFeB reaches its maximum amplitude is shown. As it is seen, this distance decreases exponentially as the damping in Py increases. The value of x_{max} indicates at which point it is optimal to cut the periodicity of Py layer to avoid back-coupling. However, the total energy transferred also decreases with damping, what is shown in figure 7(b). An increase of the α from 0.01 to 0.02 decreases A^2 from 0.4 to 0.2 for contra-directional coupling and this decreases A^2 from 0.3 to 0.15 for co-directional coupling in Py15/CoFeB bilayer. Additionally, we provide a dependence of A^2 on the damping parameter in CoFeB for the damping parameter in Py fixed to 0.01. The dependence follows exponential decay of efficiency with the damping and it is qualitatively similar to the dependence for permalloy. Note, that the efficiency A^2 is better for for contra-directional coupling than for co-directional coupling and for the same value of α in spite of the fact that the coupling coefficient is smaller. This is mainly, because of the lower resonant frequency and wavenumber for contra-directional coupling, which leads to the lower effective damping (equation (11)).

Next, we have analized how the energy transfer efficiency coefficient depends on the separation between layers and the depth of thickness modulation in permalloy layer. Figure 8(a) shows the values of A^2 for the value of grooves in Py fixed to $c = 15$ nm. The value of A^2 reaches maximum of about 0.3 and 0.4 for the co-directional and contra-directional couplings, respectively, for the distance between the layers of 200 nm. Figure 8(b) shows that the efficiency of energy transfer between layers (fixed distance of 200 nm) increase with the increase of the thickness modulation. That strictly reflects the dependence of coupling coefficient κ on the layers separation and thickness modulation.

Finally, we analyzed with MuMax3 the transmission of the broadband signal (wave packet) excited in CoFeB to the Py layer. The results are shown in figures 3(c) and (d) by the color map. Very good agreement with the previous computations has been obtained, proving the correctness of the investigations. Moreover, as indicated by the intensity map, the signal transmits between the layers only at the vicinity of the crossings. That suggests, a system may operate not only as a short-wavelength SW generator, but also as a frequency filter.

4. Conclusions

In conclusion, we have shown resonant energy exchange between the two SWs modes propagating in two different ferromagnetic layers in the Damon–Eshbach configuration. We demonstrated numerically, that it is

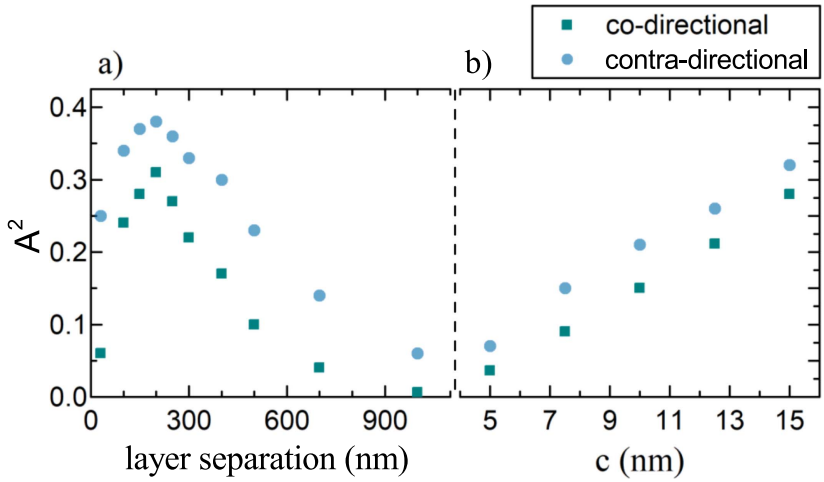

Figure 8. (a) The dependencies of the efficiency coefficient on (a) the separation between Py and CoFeB layers and (b) depth of thickness modulation for co-directional and contra-directional crossings.

possible to utilize this effect to excite short SWs from the long SWs or to filter particular resonant frequency from the wave packet from one layer to another layer. The other interesting option would be to transfer the whole wave packet from the one medium to another. This effect could be achieved also in the finite-size waveguides by optimizing their dispersion relation to obtain broadband resonance, which will be promissing for development magnonics applications.

Acknowledgments

The study has received financial support from the National Science Centre of Poland under grants UMO-2012/07/E/ST3/00538 and the EU's Horizon 2020 Research and Innovation Program under Marie Sklodowska-Curie Grant Agreement No. 644348 (MagIC).

ORCID iDs

Mateusz Zelent https://orcid.org/0000-0001-7843-611X

References

[1] Wong H-S P, Lee C-S and Luo J 2018 CMOS Technology Scaling Trend http://nano.stanford.edu/cmos-technology-scaling-trend
[2] Theis T N and Wong H-S P 2016 *Comput. Sci. Eng.* **19** 41
[3] Kruglyak V V, Demokritov S O and Grundler D 2010 *J. Phys. D: Appl. Phys.* **43** 264001
[4] Stamps R L *et al* 2014 *J. Phys. D: Appl. Phys.* **47** 333001
[5] Grundler D 2016 *Nat. Nanotechnol.* **11** 407
[6] Khitun A, Bao M and Wang K L 2010 *J. Phys. D: Appl. Phys.* **43** 264005
[7] Lenk B, Ulrichs H, Garbs F and Munzenberg M 2011 *Phys. Rep.* **507** 107
[8] Chumak A V, Vasyuchka V I, Serga A A and Hillebrands B 2015 *Nat. Phys.* **11** 453
[9] Demidov V E, Kostylev M P, Rott K, Mnchenberger J, Reiss G and Demokritov S O 2011 *Appl. Phys. Lett.* **99** 082507
[10] Au Y, Ahmad E, Dmytriiev O, Dvornik M, Davison T and Kruglyak V V 2012 *Appl. Phys. Lett.* **100** 182404
[11] Davies C S and Kruglyak V V 2016 *IEEE Trans. Magn.* **52** 7378955
[12] Yu H, Duerr G, Huber R, Bahr M, Schwarze T, Brandl F and Grundler D 2013 *Nat. Commun.* **4** 2702
[13] Sklenar J, Bhat V S, Tsai C C, Delong L E and Ketterson J B 2012 *Appl. Phys. Lett.* **101** 052404
[14] Yu H, d'Allivy Kelly O, Cros V, Bernard R, Bortolotti P, Anane A, Brandl F, Heimbach F and Grundler D 2016 *Nat. Commun.* **7** 11255
[15] Maendl S, Stasinopoulos I and Grundler D 2017 *Appl. Phys. Lett.* **111** 12403
[16] Hämäläinen S J, Brandl F, Franke K J, Grundler D and Dijken S Van 2017 *Phys. Rev. Appl.* **8** 014020
[17] Graczyk P, Kłos J and Krawczyk M 2017 *Phys. Rev.* B **95** 104425
[18] Graczyk P and Krawczyk M 2017 *Phys. Rev.* B **96** 024407
[19] Van de Wiele B, Hämäläinen S J, Baláž P, Montoncello F and van Dijken S 2016 *Sci. Rep.* **6** 21330
[20] Davies C S, Sadovnikov A V, Grishin S V, Sharaevsky Y P, Nikitov S A and Kruglyak V V 2015 *IEEE Trans. Magn.* **51** 1
[21] Sadovnikov A V, Beginin E N, Morozova M A, Sharaevskii Y P, Grishin S V, Sheshukova S E and Nikitov S A 2016 *Appl. Phys. Lett.* **109** 42407
[22] Sadovnikov A V, Beginin E N, Sheshukova S E, Romanenko D V, Sharaevskii Y P and Nikitov S A 2015 *Appl. Phys. Lett.* **107** 202405
[23] Sadovnikov A V, Odintsov S A, Beginin E N, Sheshukova S E, Sharaevskii Y P and Nikitov S A 2017 *IEEE Trans. Magn.* **53** 1
[24] Fernández-Pacheco A, Streubel R, Fruchart O, Hertel R, Fischer P and Cowburn R P 2017 *Nat. Commun.* **8** 15756

[25] Morozova M A, Sharaevskaya A Y, Sadovnikov A V, Grishin S V, Romanenko D V, Beginin E N, Sharaevskii Y P and Nikitov S A 2016 *J. Appl. Phys.* **120** 223901
[26] Morozova M A, Sharaevskaya A Y, Matveev O V, Beginin E N and Sharaevskii Y P 2016 *Phys. Wave Phenom.* **24** 1
[27] Mruczkiewicz M, Graczyk P, Lupo P, Adeyeye A, Gubbiotti G and Krawczyk M 2017 *Phys. Rev.* B **96** 104411
[28] Sasaki H and Mikoshiba N 1979 *Electron. Lett.* **15** 172
[29] Koike T 1980 *Ultrasonics Symposium* (Piscataway, NJ: IEEE) pp 552–6
[30] Alferness R 1981 *IEEE J. Quantum Electron.* **17** 946
[31] Tien P K 1977 *Rev. Mod. Phys.* **49** 361
[32] Wang Q, Pirro P, Verba R, Slavin A, Hillebrands B and Chumak A V 2018 Reconfigurable nano-scale spin-wave directional coupler *Sci. Adv.* **4** e1701517
[33] Mruczkiewicz M, Krawczyk M, Sakharov V K, Khivintsev Y V, Filimonov Y A and Nikitov S A 2013 *J. Appl. Phys.* **113** 093908
[34] Vansteenkiste A, Leliaert J, Dvornik M, Helsen M, Garcia-Sanchez F and Waeyenberge B V 2014 *AIP Adv.* **4** 107133
[35] Yariv A and Yeh P 2003 *Optical Waves in Crystals* (New York: Wiley) pp 177–201
[36] Zhang K and Li D 2008 *Electromagnetic Theory for Microwaves and Optoelectronics* (Berlin: Springer) pp 450–61
[37] Huang W-P 1994 *J. Opt. Soc. Am.* **11** 963
[38] Stancil D D and Prabhakar A 2009 *Spin Waves* (Berlin: Springer) ch. Appendix C
[39] Henry Y, Gladii O and Bailleul M 2016 arXiv:1611.06153 [cond-mat.mes-hall]